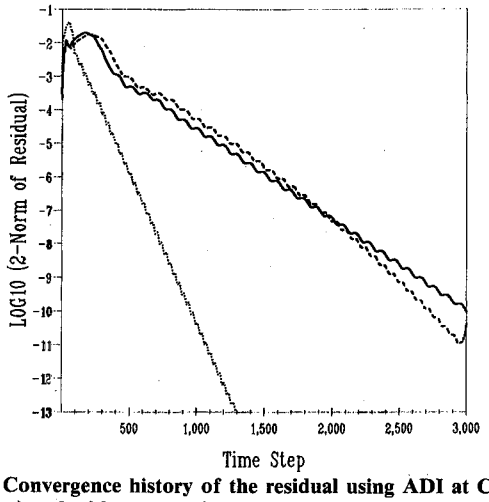

Fig. 1 Convergence history of the residual using ADI at CFL = 13 (solid line) and with an adaptive time step at CFL = 20 (dashed line) and CGS-ADI at CFL = 40 (dotted line).

Table 1 Computational efficiency of the CGS-ADI code and of the ADI code

Test case	Code	Number of steps	CPU time, s
1	CGS-ADI	600	1643
1	ADI	1800	2813
2	CGS-ADI	700	1955
2	ADI	2600	4105

The results on the second test cases show the same qualitative behavior. However, the convergence of the ADI code to the steady state is significantly slower than in the first case, probably due to the presence of greater shocks.

Table 1 summarizes the computational costs for obtaining a converged solution (residual L_2 norm smaller than 10^{-8}) with the two codes. All of the relevant computational kernels of both codes run at about 20 Mflops on one vector processor of the IBM 3090 model 600E. The greater cost per time step of the CGS-ADI code is largely compensated, on both problems, by its faster convergence rate. Indeed, for both convergence criteria CGS-ADI required about 1.7 times less CPU time than ADI on the first problem and about 2.1 less CPU time on the second problem.

Conclusion

The numerical stability bounds of implicit schemes based on the Beam-Warming linearization procedure are adversely affected by the factorization errors introduced by ADI splitting methods. In order to accelerate the convergence to the steady state, the use of large time steps may be exploited more effectively when the unfactored form of the implicit-step operator is retained. In two-dimensional problems the CGS-ADI iterative algorithm is very efficient for solving the unfactored implicit-step operator, and the implemented code was found to be significantly faster than an ADI code employing block-tridiagonal factors. On two transonic airfoil test cases the CGS-ADI code required, respectively, 1.7 and 2 times less CPU time than the ADI code to obtain a converged solution.

References

[1]Beam, R. M., and Warming, R. F., "An Implicit Finite-Difference Algorithm for Hyperbolic Systems in Conservation-Law Form," *Journal of Computational Physics*, Vol. 22, No. 1, 1976, pp. 87–110.

[2]Pulliam, T. H., "Euler and Thin Layer Navier Stokes Codes: ARC2D, ARC3D," *Notes for the Computational Fluid Dynamics User's Workshop*, Univ. of Tennessee Space Institute, Tullahoma, TN, 1984.

[3]Sonnenveld, P., "CGS, a Fast Lanczos-Type Solver for Nonsymmetric Linear Systems," *SIAM Journal of Scientific and Statistical Computing*, Vol. 10, No. 1, 1989, pp. 36–52.

[4]Jameson, A., Schmidt, W., and Turkel, E., "Numerical Solutions of the Euler Equations by Finite Volume Methods Using Runge-Kutta Time-Stepping Schemes," AIAA Paper 81-1259, 1981.

[5]Fletcher, R., "Conjugate Gradient Methods for Indefinite Systems," *Lecture Notes in Mathematics 506*, Springer-Verlag, Berlin, Germany 1976, pp. 73–89.

[6]Saad, Y., Schultz, M.H. "GMRES: a Generalized Minimal Residual Algorithm for Solving Nonsymmetric Linear Systems," *SIAM Journal of Scientific and Statistical Computing*, Vol. 7, No. 3, 1986, pp. 856–869.

[7]Wigton, L. B., Yu, N. J., and Young, D. P., "GMRES Acceleration of Computational Fluid Dynamics Codes," AIAA Paper 85-1494, 1985.

Study of Wake Optical Properties

N. Gerber* and R. Sedney†
U.S. Army Ballistic Research Laboratory, Aberdeen Proving Ground, Maryland 21005

An experiment[1] and associated theoretical study[2] were performed to study the optical transmittal properties of the turbulent wake behind a supersonic projectile. The experiment consisted of taking nearly end-on shadowgraphs of the wake and projectile. A projectile was fired toward a photographic film oriented normal to the trajectory. A small turning mirror located near the trajectory reflected a pulsed, diverging beam of laser light (wavelength 6943 Å) upstream through the wake toward the projectile at a predetermined time. This short-duration pulse (< 100 ns) imprinted a shadow image on the film before the projectile pierced it. The projectile shadow was centered off the trajectory, and the piercing hole left enough of it so that more than half of the boundary appeared on the film, as seen in a typical shadowgraph, Fig. 1.

The projectile shadowgraphs were then measured. In every test, the shadow with wake was significantly larger than that computed by geometrical projection, indicating that the wake acted as a diverging lens.

Geometrical optics was the theoretical approach employed to determine the projectile shadow. The differential equations for propagation of light rays in a nonhomogeneous medium[3] were integrated for the light traveling upstream from the pulsed point source. Those rays that grazed the base of the projectile were then extended in straight lines from base to screen in the directions that they had at the base, thus forming the theoretical shadow. The equations to be integrated are

$$\frac{\partial F}{\partial x} - \frac{d(\partial F/\partial \dot{x})}{dz} = 0$$

$$\frac{\partial F}{\partial y} - \frac{d(\partial F/\partial \dot{y})}{dz} = 0$$

where

$$\dot{x} \equiv \frac{dx}{dz}, \qquad \dot{y} \equiv \frac{dy}{dz}$$

$$F(z,x,y,\dot{x},\dot{y}) \equiv n(x,y,z)(\dot{x}^2 + \dot{y}^2 + 1)^{1/2}$$

The x, y plane is normal to the trajectory, which coincides with the z axis; the light source is located on $y = 0$. The index

Received Feb. 20, 1990; revision received May 5, 1990; accepted for publication May 21, 1990. This paper is declared a work of the U.S. Government and is not subject to copyright protection in the United States.

*Aerospace Engineer, Launch and Flight Division. Member AIAA.
†Research Scientist, Launch and Flight Division. Member AIAA (deceased).

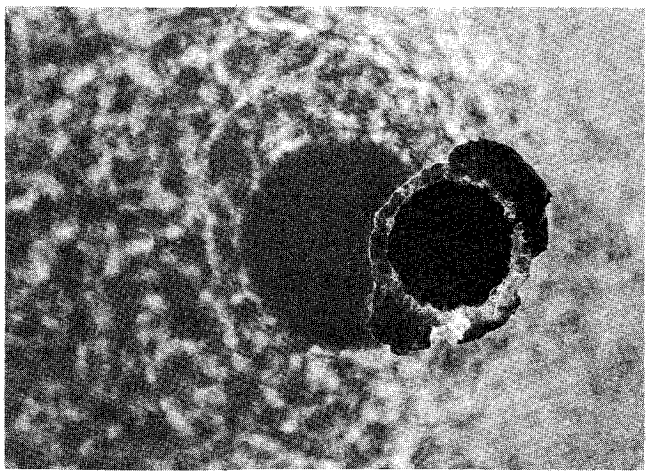

Fig. 1 Typical end-on shadowgraph of projectile.

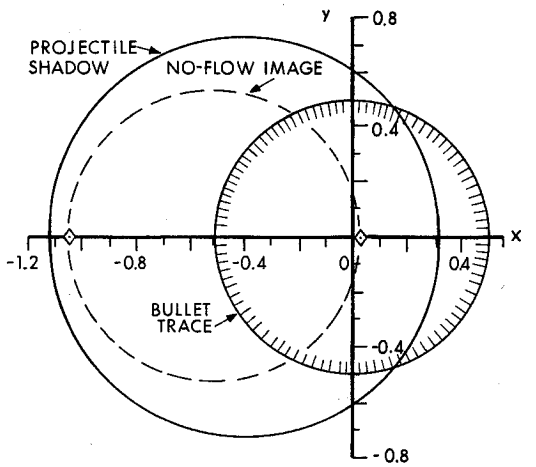

Fig. 2 Calculated end-on shadow of projectile.

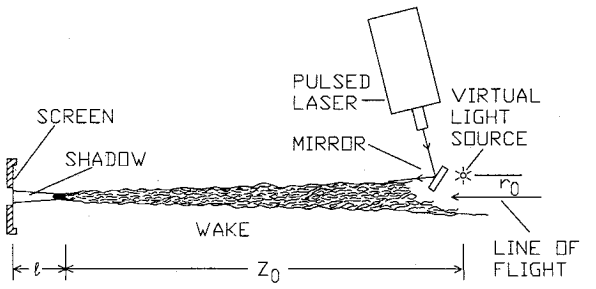

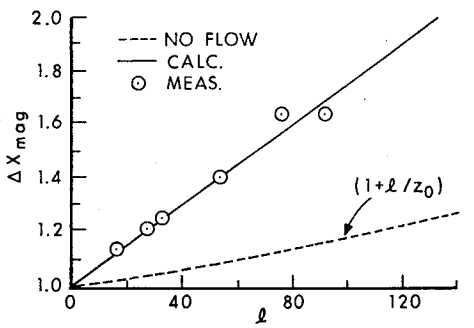

Fig. 3 Magnification vs projectile location for fixed light source and screen: $r_o = 5.75$, $z_o = 646.4 - l$.

of refraction $n(x, y, z)$, was obtained from the gas density ρ in the flowfield by the Dale-Gladstone law (where ∞ signifies ambient conditions):

$$n = n_\infty + (n_\infty - 1)[(\rho/\rho_\infty) - 1]$$

Only the refractive effect of the mean density was considered; optical effects of the fluctuating part of ρ were omitted.

Crucial to the solution was the presence of accurate data for the wake density. A semiempirical model developed by Finson[4] was used. (A summary of the equations arising from it is given in Ref. 2.) In this model, the mean velocity on the axis beyond the rear stagnation point is specified as a universal function of downstream distance. Conservation of energy is then used to relate the velocity and temperature on the axis. Approximate radial profiles are specified for the temperature from similarity arguments. The density field is then obtained with the perfect gas law, with the additional approximation that the pressure is constant, equal to the ambient value. This model is expected to be applicable for the parameters of the experiments employed in its derivation, namely, for $M_\infty \leq 5$, for Reynolds numbers in the range $10^4 - 10^6$, and for a wide variety of body shapes.

Figure 2 shows a typical shadow calculation at the screen. The computed projectile shadow is seen to be almost circular. This case ($l = 52.9$, see Fig. 3) is one of six rounds fired for fixed light source and screen; the magnifications Δx_{mag} for these rounds, both measured and computed, are plotted in Fig. 3, where distances are nondimensionalized by the diameter of the projectile base, $D = 0.782$ cm. The virtual light source created by the turning mirror is indicated in this figure. The magnification Δx_{mag} is defined as the nondimensionalized distance between the two intercepts of the projectile shadow with the x axis. Parameters for these cases required by the model are $n_\infty = 1.0002780$, projectile drag coefficient $C_D = 0.316$, projectile Mach number $M_\infty = 2.41$, ratio of specific heats of ambient air $\gamma = 1.4$, and ratio of mean wall temperature to ambient temperature $T_w/T_\infty = 1.10$.

Measured and theoretical magnifications show agreement to within 6% for all firings. This agreement is notably better than one should expect, considering the simplifications of the theory and the experimental uncertainties. (Reference 1, an exploratory report, does not provide estimates of experimental errors.) It is noted that Δx_{mag} varies linearly with l, in contrast to the Δx_{mag} of geometrical projection. One would conclude from the experiments (at least for 600 calibers of wake) that scattering and diffusion of light by turbulent fluctuations have a small effect, compared to refraction, on the propagation of light through the wake of a projectile and, furthermore, that the wake acts optically as a diverging lens for light rays traveling nearly lengthwise through it.

Acknowledgments

The authors gratefully acknowledge the help of J. M. Bartos, who programmed and performed the computations. The experiments were originated by G. D. Kahl and were performed by D. B. Sleator and D. D. Shear.

References

[1]Kahl, G. D., Sleator, D. B., and Shear, D. D., "Experiments on Wake Optical Properties," U.S. Army Ballistic Research Lab., Aberdeen Proving Ground, MD, BRL-MR-2496, AD B005619, July 1975.

[2]Sedney, R., Gerber, N., and Bartos, J. M., "Tracing of Light Rays along a Projectile Wake," U.S. Army Ballistic Research Lab., Aberdeen Proving Ground, MD, TR-ARBRL-TR-02119, AD A064099, Nov. 1978.

[3]Born, M., and Wolf, E., *Principles of Optics,* Pergamon, New York, 1980, Appendix I, p. 733.

[4]Finson, M. L., "Density Distributions in Supersonic Projectile Wakes," Physical Sciences, Inc., Andover, MA, Rept. PSI TR-66, BRL Contract DAADO5-76-MD111, 1976.